



32 potential to substantially reduce uncertainty in palaeoclimate reconstructions, allowing for unbiased
33 temperature estimates from sparse data.

34 **Keywords**

35 Palaeoclimate, latitudinal temperature gradients, temperature proxies, Eocene, spatial bias, Bayesian

36 **Introduction**

37 Understanding the long-term evolution of Earth's climate system and contextualising current global
38 warming relies on accurate reconstructions of past climates (Royer et al., 2004; Burke et al., 2018; Tierney
39 et al., 2020). Recent advances in the synthesis of palaeoclimate data (e.g. Veizer and Prokoph, 2015; Hollis
40 et al., 2019; Song et al., 2019; Grossman and Joachimski, 2022; Judd et al., 2022) are offering
41 unprecedented insights into the complex and dynamic nature of the Earth's climate system, yet a
42 fundamental challenge remains: the proxy record of past climates is spatially incomplete and afflicted by
43 imperfect preservation and uneven sampling (Judd et al., 2020; Jones and Eichenseer, 2022; Judd et al.,
44 2022).

45 Whilst geochemical proxy data can provide robust estimates of palaeotemperature at local scales, recent
46 work has demonstrated that spatial biases in the geochemical proxy record can lead to spurious estimates
47 of regional (e.g. latitudinal temperature gradients) and global temperatures (Judd et al., 2020; Jones and
48 Eichenseer, 2022). Principally, this can be driven by two factors: (1) missing data for some regions (e.g. no
49 high-latitude data); or (2) overrepresentation of other regions (e.g. a high proportion of samples from
50 tropical areas). The latter can be addressed through the down-sampling of data or restricting analyses to
51 specific regions (e.g. Song et al., 2019). However, in order to robustly infer regional or global-scale patterns
52 from an incomplete record, spatial gaps must ultimately be bridged. One common approach, which requires
53 no additional computation, is the spatial visualisation of proxy-derived temperatures against latitude,
54 showing broad latitudinal temperature trends (Hollis et al., 2019; Vickers et al., 2021). Interpolation is also
55 sometimes used to bridge spatial gaps in palaeoclimate data (Taylor et al., 2004), taking advantage of the
56 autoregressive nature of climatic data: much of the information on the climate of any given location is
57 contained in the climate data of nearby locations (Reynolds and Smith, 1994). Adding to this, some proxy-
58 based reconstructions use statistical modelling to infer palaeoclimatic patterns. For example, polynomial
59 regression (Bijl et al., 2009) and cosine functions (Inglis et al., 2020) have been used to reconstruct
60 latitudinal temperature gradients, and 2D-reconstructions of surface temperatures have been created with
61 Gaussian process regression (Inglis et al., 2020). These approaches work well for interpolating relatively



62 densely-sampled data, but the absence of constraints on the modelled parameters means that such models
63 can produce unrealistic temperature estimates when extrapolating from sparse data. Statistical modelling in
64 a Bayesian framework can help overcome this problem by requiring the explicit specification of priors for
65 the model parameters, which can be used to express physical constraints (Chandra et al., 2021).

66 Spatial gaps in the palaeoclimate record can also be addressed through the integration of additional data.
67 For example, lithological and fossil data can be used to infer past climatic conditions based on analogous
68 modern sediments (Chandra et al., 2021), or based on the premise that the climatic requirements of ancient
69 taxa, biological traits, or ecological communities were similar to those of their nearest modern relatives
70 (Peppe et al., 2011; Royer, 2012; Salonen et al., 2019). Despite this potential, the integration of geochemical
71 proxy data with other sources of information (e.g. ecological data) has rarely been realised in a rigorous,
72 quantitative framework (Burgener et al., 2023).

73 Here, we present a novel Bayesian hierarchical model that combines quantitative proxies and ecological
74 constraints into a fully quantitative model of the latitudinal gradient of sea surface temperatures, bridging
75 spatial gaps in sparsely sampled climate data. This model expands upon existing, spatially explicit
76 palaeoclimatic reconstructions by allowing for the integration of (1) prior information based on physical
77 principles and the observed modern sea surface temperature distribution, and of (2) geochemical and
78 ecological climate proxies in a common, quantitative framework. We use a generalised logistic function to
79 accurately infer the shape of the temperature gradient despite a patchy latitudinal coverage, and test the
80 robustness of this method using down-sampled, simulated temperature gradients.

81 We apply this model to the record of the early Eocene climatic optimum (EECO), combining a compilation
82 of geochemical proxies (Hollis et al., 2019), mangrove communities (Popescu et al., 2021), and coral reefs
83 (Zamagni et al., 2012), using a nearest-living-relative approach (e.g. Greenwood et al., 2017) to establish
84 broad temperature ranges for the ecological data. We choose the EECO to demonstrate the application of
85 the model due to its significance as the interval with the warmest sustained temperatures of the Cenozoic
86 (Pross et al., 2012), rendering it a potential analogue for extreme climate warming scenarios (Burke et al.,
87 2018). Our integrative approach allows us to shed new light on the long-standing dispute on the steepness
88 of the early Eocene temperature gradient (Table 1; Sloan and Barron, 1990; Markwick, 1994; Huber and
89 Caballero, 2011; Tierney et al., 2017; Inglis et al., 2020).

90 Table 1: Inferred latitudinal sea surface temperature (SST) gradients for the early Eocene (EE) or the EECO,
91 as shown in earlier, proxy-based studies. For comparison, a gradient derived from an atmosphere-ocean
92 general circulation model (GCM) ensemble is also shown.



Source	Time	Gradient	Type_of_gradient	Model	Proxy_system
Bijl et al. (2009)	EE	7	equator - polar circle	2 nd order polynomial	TEX ₈₆ , UK ₃₇ ^{K'}
Keating-Bitoni et al. (2011)	EECO	13	equator - polar circle	2 nd order polynomial	TEX ₈₆ , MBT/CBT, Δ ₄₇ , Mg/Ca, δ ¹⁸ O
Tierney et al. (2017)	EE	12	equator - polar circle	Gaussian function	TEX ₈₆
Cramwinckel et al. (2018)	EECO	21 (±1)	equator - deep water	-	TEX ₈₆ , Δ ₄₇ , Mg/Ca, δ ¹⁸ O, deepwater δ ¹⁸ O
Evans et al. (2018)	EE	20 (±3)	tropics - deep water	-	Δ ₄₇ , deepwater Mg/Ca
Pross et al. (2012), as shown in Tierney et al. (2017)	EE	26	equator - polar circle	climate model ensemble (GCM)	none (GCM simulations)

93 **Materials & Methods**

94 **Geochemical data**

95 Geochemical climate proxy data were extracted from a latest Paleocene and early Eocene compilation
 96 (Hollis et al., 2019). This compilation provides data on four different geochemical proxies for
 97 reconstructing seawater temperature: δ¹⁸O, Δ₄₇, Mg/Ca and TEX₈₆. For our analyses, this dataset was
 98 restricted to the EECO (defined as 53.8 – 49.1 Ma) and samples from the continental shelf. Recrystallised
 99 δ¹⁸O samples were also excluded as secondary diagenetic calcite precipitated after deposition can bias
 100 isotope measurements and offset temperature values (Schrag, 1999). This filtering resulted in most δ¹⁸O
 101 samples being excluded from the dataset (retaining 8 out of 152). After data filtering, 308 geochemical
 102 proxy samples from 23 locations remained. For a detailed description of each proxy see Hollis et al. (2019).

103 **Ecological data**

104 **Coral reefs.** Today, shallow warm-water coral reefs are limited to tropical and subtropical latitudes (~34° N
 105 – 32° S), with minimum sea surface temperature tolerances (~18°C) being the primary constraint on this
 106 distribution (Johannes et al., 1983; Kleypas et al., 1999; Yamano et al., 2001). As coral reefs reside at the
 107 upper thermal limit of the oceans today, their maximum sea surface temperature tolerance is less well-



108 constrained, with some studies suggesting up to 35.6°C in the geological past (Jones et al., 2022).
109 Nevertheless, coral reefs have frequently been recognised as tracers of past (sub-)tropical conditions
110 (Ziegler et al., 1984; Kiessling, 2001). During the Eocene, coral communities and reefs expanded across
111 tropical and temperate latitudes, with communities found up to palaeolatitudes of 43 ° N (Zamagni et al.,
112 2012). Using a compilation of Paleocene – early Eocene coral reefs and community localities (Zamagni et
113 al., 2012), we generated quantitative sea surface temperature estimates for the ECCO. To do so, we
114 extracted localities from the compilation that are inferred to be Ilerdian (early Eocene) coral reefs, and that
115 could be confidently assigned to the EECO. We excluded coral knobs and coral-bearing mounds which
116 might have broader climatic limits than warm-water coral reef ecosystems. This filtering resulted in four
117 unique coral reef localities remaining for the EECO, all of which conform to the modern latitudinal range
118 of coral reefs (<34° N). Subsequently, we used statistically derived temperature limits (minimum = 21°C,
119 average = 27.6°C, maximum = 29.5°C) from the published literature (Kleypas et al., 1999) to define a
120 normal probability distribution of potential temperature values for coral reef localities. This normal
121 probability distribution was defined with a mean of 27.6 and a standard deviation of 2.125, placing 97.5%
122 of the probability density above the minimum. As the distribution of modern corals is skewed towards
123 warmer temperatures, this approach results in 16.5% of the probability being placed on temperatures >
124 29.5°C, allowing for the possibility that Eocene coral reefs were adapted to warmer conditions than present-
125 day coral reefs.

126 **Mangroves.** Mangroves are distributed throughout the tropics and subtropics today. While factors besides
127 sea surface temperatures (SST) influence the distribution of mangroves, empirical, lower temperature limits
128 have been established for the genera *Avicennia* (15.6°C) and *Rhizophora* (20.7°C) (Quisthoudt et al., 2012).
129 Both *Avicennia* and members of the Rhizophoraceae family were widespread and co-occurred across
130 tropical and temperate latitudes in the early Eocene. Only *Avicennia*, however, occurred at polar latitudes
131 (Suan et al., 2017; Popescu et al., 2021). Assuming that Eocene members of these mangrove taxa conform
132 to similar climatic requirements as their modern relatives, the presence and absence of *Avicennia* and
133 Rhizophoraceae pollen can be used as a palaeotemperature indicator. For this analysis, published mangrove
134 occurrence data were taken from Popescu et al. (2021), and converted to quantitative temperature estimates.
135 From this data, we identify two types of pollen assemblages which we ascribe different temperature
136 distributions:

137 1) *Avicennia*-only assemblages ($n = 2$): the absence of Rhizophoraceae is indicative of temperatures
138 being between 15.6°C (lower temperature limit of *Avicennia*) and 20.7°C (lower temperature limit
139 of *Rhizophora*). However, a value of 22.5°C is ascribed as the upper temperature limit here as
140 *Rhizophora* is rare below this temperature. We define the *Avicennia*-only temperature distribution
141 as a normal distribution with a mean of 19.05 and a standard deviation of 1.725, resulting in 95%
142 of the probability density being placed within the temperature limits.



143 2) *Avicennia* and Rhizophoraceae assemblages ($n = 5$): the presence of both groups suggests that
144 the locality should have a minimum temperature of 20.7°C (lower temperature limit of
145 *Rhizophora*). As the upper thermal limits of *Avicennia* and *Rhizophora* are not well established
146 in Quisthoudt et al. (2012), we assign the same maximum temperature limits (29.5°C) as coral
147 reef localities, because mangroves are also widely distributed throughout tropical regions.
148 Consequently, we define the temperature distribution for this locality as a normal distribution
149 with a mean of 25.1 and a standard deviation of 2.2, with 95% probability density within the
150 temperature limits.

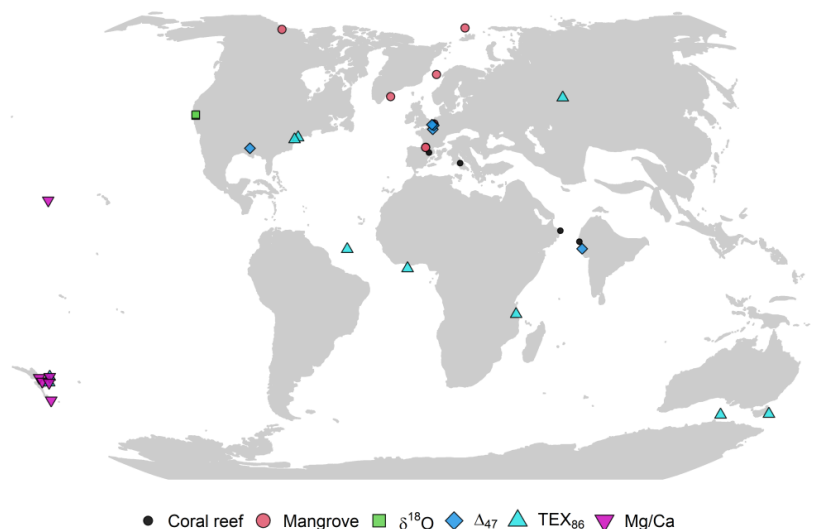


Figure 1: Palaeogeographic distribution of the geochemical and ecological data compilation used in this study. Map is presented in the Robinson projection (ESRI:54030).

151 Palaeogeographic reconstruction

152 The palaeogeographic distribution of geochemical and ecological data was reconstructed using the Merdith
153 et al. (2021) plate rotation model via the palaeoverse R package (version 1.2.0, Jones et al., 2023). The
154 midpoint age of the EECO (51.2 Ma), along with the present-day coordinates of geochemical and ecological
155 data, were used for palaeogeographic reconstruction.

156 Bayesian framework

157 **Model structure.** We model the mean temperature (μ) at location j as a function of absolute latitude
158 ($abs(l)$) with a logistic regression (also known as “growth curve” or “Richard’s curve”) of the form:

$$159 \mu_j \sim N(v_j, \sigma), \quad (1)$$



160
$$v_j = A + \frac{K - A}{e^{B(\text{abs}(l_j) - M)}}, \quad j = 1, \dots, n, \quad (2)$$

161 where A and K denote the lower and upper asymptote, respectively, M specifies the latitude of maximal
162 growth, i.e. the latitude around which temperature falls most steeply with latitude, B denotes the growth
163 rate, σ denotes the residual standard deviation, and n denotes the number of locations.

164 We infer μ_j from m individual temperature observations $t_{i=1,\dots,m}$, derived from geochemical data, at
165 location j as

166
$$t_{i,j} \sim N(\mu_j, \sigma_j), \quad i = 1, \dots, m, \quad (3)$$

167 where m is the number of observations at each location, and σ_j is the estimated standard deviation of the
168 temperatures at location j .

169 Similarly, μ_j is inferred for locations with ecological proxies from the associated normal temperature
170 distributions with a given mean and standard deviation, $t_{\mu,j}$ and $t_{\sigma,j}$, as

171
$$t_{\mu,j} \sim N(\mu_j, t_{\sigma,j}). \quad (4)$$

172 This structure implies that μ_j is not fixed at the mean proxy temperature at location j , but is drawn towards
173 the overall logistic regression curve, i.e. towards v_j . The pull towards v_j tends to be strong when m is low,
174 when the observations $t_{i=1,\dots,m,j}$ are scattered, i.e. σ_j is high, and/or when the overall standard deviation σ
175 is low. In practice, this has the desirable consequence that locations with few observations and large
176 temperature differences between observations have less influence on the overall regression than well-
177 sampled locations with consistent reconstructed temperatures.

178 **Priors.** In a Bayesian framework, priors need to be placed on the unknown parameters of a model. We
179 placed weakly informative, conjugate inverse-gamma priors on σ and $\sigma_{j=1,\dots,n}$:

180
$$\sigma \sim \sqrt{\text{Inv-Gamma}\left(\alpha + \frac{n}{2}, \beta + 0.5 \times (\mu_j - v_j)\right)}, \quad j = 1, \dots, n, \quad (5)$$

181
$$\sigma_j \sim \sqrt{\text{Inv-Gamma}\left(\alpha + \frac{m}{2}, \beta + 0.5 \times (t_{i,j} - \mu_j)\right)}, \quad i = 1, \dots, m, \quad j = 1, \dots, n. \quad (6)$$

182 We set $\alpha = \beta = 1$, allowing these priors to be quickly overwhelmed by the data as n and m increase, as
183 we have little *a priori* knowledge of these parameters.



184 In contrast, we put informative priors on the regression coefficients A , K , M and B , based on physical
185 principles, and loosely based on the modern climate system:

186 **A.** Predicted seawater surface temperatures are not allowed to be $\ll -2^\circ\text{C}$, the freezing point of sea water.
187 The highest prior density of A is placed around 0°C , and it slowly tapers off towards higher temperatures.
188 This shape is achieved by placing a skew-normal prior on the lower asymptote, specified as

$$189 \quad A \sim SN(\xi = -3.0, \omega = 12, \alpha_{SN} = 30), \quad (7)$$

190 where ξ , ω , and α_{SN} are the location, scale and shape parameters.

191 **K.** Input of solar energy decreases from the tropics to the poles. Hence, the latitudinal temperature gradient
192 is broadly negative, i.e. temperature decreases with absolute latitude. This is achieved by setting $K \geq A$.
193 The prior on the upper asymptote K is a truncated normal distribution with the mean set to K of the modern
194 SST gradient, with a broad standard deviation:

$$195 \quad K \sim TN(\mu_{TN} = 28, \sigma_{TN} = 10, \alpha_{TN} = A, \beta_{TN} = \infty) \quad (8)$$

196 The distribution is truncated to the left at $\alpha_{TN} = A$, but not truncated to the right (β_{TN}).

197 **M.** The steepness of the gradient is presumed to be highest in mid-latitudes; this is expressed with a normal
198 prior on M with the mean set to 42, i.e. M of the modern SST gradient, and a moderately wide standard
199 deviation of 10:

$$200 \quad M \sim N(42, 10) \quad (9)$$

201 **B.** The steepness or growth rate B of the gradient is constrained to be ≥ 0 and to not be exceedingly high,
202 as oceanic and atmospheric heat transfer is bound to limit very abrupt SST changes across latitudes on a
203 global scale. A gamma-distributed prior of the form

$$204 \quad B \sim \text{Gamma}(\alpha_G = 4.3, \beta_G = 30) \quad (10)$$

205 was placed on B . The shape and rate parameters α_G and β_G were chosen such that the highest prior density
206 is at B of the modern SST gradient, 0.11. We informed the prior distributions on M and B based on a
207 provisional model run with the modern SST data.

208 **Model validation**

209 To test whether our logistic regression model can adequately describe different latitudinal temperature
210 gradients at various sample sizes, we generated four idealised gradients that emulate potential climatic states
211 throughout Earth's geological history: extreme icehouse, icehouse, greenhouse, and extreme greenhouse



212 (Frakes et al., 1992). We then randomly sampled (1,000 iterations) these gradients using increasing sample
213 sizes (5, 10, and 20) and reconstructed the latitudinal temperature gradient using our model for each of
214 these sample sizes and gradient types. Using the same idealised gradients, we also tested whether our model
215 could accurately reconstruct latitudinal temperature gradients using the palaeogeographic distribution of
216 Eocene samples ($n = 34$), providing an empirical, exemplary distribution that captures both limited sample
217 size and skewed geographic origins of samples. To evaluate how well the model performed in
218 reconstructing the idealised gradients from limited sampling, we calculated the coefficient of determination
219 (R^2) for Bayesian regression models (Gelman et al., 2019). For every iteration from the posterior, we
220 intercepted the modelled and the idealised gradient in intervals of 1° latitude and calculated the R^2 based
221 on these values. We report the median, and 95% credible intervals (CI) of the resulting R^2 values. Here and
222 in all other instances, the 95% CI refer to the interval between the 2.5% point and the 97.5% point of the
223 samples or sampled posterior distribution.

224 To test whether our model can accurately depict the shape of the modern sea surface temperature gradient,
225 and to facilitate comparison with the Eocene gradient, we applied our model to annual sea surface mean
226 temperatures from Bio-Oracle (Assis et al., 2018), aggregated to a $1^\circ \times 1^\circ$ raster ($n = 46,131$). The R^2 for
227 the modern gradient was calculated as above (Gelman et al., 2019), comparing the modelled gradient and
228 the empirical temperature averages in 1° latitude bins. Only the medians are reported for the modern
229 gradient, as the 95% credible intervals are extremely narrow due to the high precision of the posterior
230 estimates.

231 To reconstruct the idealised gradients and the modern gradient, we used a simplified, non-hierarchical
232 version of our model, as every location is associated with only one temperature value, making the
233 hierarchical structure superfluous. To achieve this, we substituted temperature (t_j) for μ_j in Equation 1 and
234 Equation 5.

235 **Parameter estimation**

236 We estimated the posterior distributions of the model parameters using a Markov chain Monte Carlo
237 (MCMC) algorithm, written in R. Specifically, we sampled the unknown parameters A , K , M and B with
238 Metropolis-Hastings, and used Gibbs sampling to estimate all other unknown parameters (see Gilks et al.,
239 1995; Gelman et al., 2013). Posterior inference on the modern gradient is based on four chains with 60,000
240 iterations each, 10,000 of which were discarded as burn-in. Every 10th iteration was retained, resulting in
241 a total of 20,000 iterations with low autocorrelation. The re-sampled, simulated gradients were modelled in
242 one chain with 10,000 iterations for each of the 1,000 random samples. 5,000 iterations each were discarded
243 as burn-in, and every 25th iteration was kept, resulting in a total of 200,000 iterations across all 1,000 model



244 runs. For the simulated gradients with an Eocene sampling distribution, a single chain with 250,000
245 iterations was used, thinned to 10,000 iterations after burn-in. For the Eocene model, we ran four chains
246 with 600,000 iterations each, discarding 100,000 as burn-in and keeping every 100th iteration, as the
247 hierarchical model structure results in higher autocorrelation of the chains. The Eocene posterior inference
248 is thus based on a total of 20,000 iterations with low autocorrelation (effective multivariate sample size for
249 A , K , M and B is $> 18,000$). Trace plots of the MCMC chains indicate convergence and good mixing of the
250 chains (Fig. S1).

251 **Processing of model results**

252 modelled sea surface temperature estimates were generated with Equation 2, calculating the sea surface
253 temperatures at any latitude with the parameter estimates of each iteration from the posterior. The median
254 and 95% CI of temperatures were then taken from all temperature estimates obtained at the latitudes of
255 interest.

256 The latitudinal gradient is calculated as the difference between the modelled temperature at the equator (0°
257 latitude) and at the poles (90° absolute latitude). To facilitate comparison with earlier estimates, we also
258 calculate the gradient with the temperature at the polar circle (66.6° absolute latitude) being used instead of
259 the temperature at the poles. Given the sigmoidal shape of the modern as well as the Eocene gradient (see
260 Fig. 4), these results are broadly comparable to a gradient inferred from the zonal average of equatorial and
261 high-latitude temperatures, as has been done in some earlier studies (Evans et al., 2018).

262 Differences between Eocene and modern temperatures at a certain latitude were calculated by randomly
263 pairing all iterations of the posterior from the Eocene and modern temperature gradient model, calculating
264 the Eocene and modern temperature using the respective iterations, taking the difference, and then
265 calculating the median (95% CI) from all pairs of iterations.

266 Global average temperatures with 95% credible intervals were calculated by taking the weighted mean of
267 the median (95% CI) of temperature estimates in 1° latitudinal bins. The weights were set to the proportion
268 of global surface area in each latitudinal bin, i.e. decreasing with increasing latitude as:

$$269 \quad \text{weights} = \sin(\alpha_{1,i}) - \sin(\alpha_{2,i}), \quad (11)$$

270 where α_1 is the upper, and α_2 is the lower latitudinal boundary of bin i , i.e. we approximated the shape of
271 the globe as a spheroid.



272 Results

273 Model validation

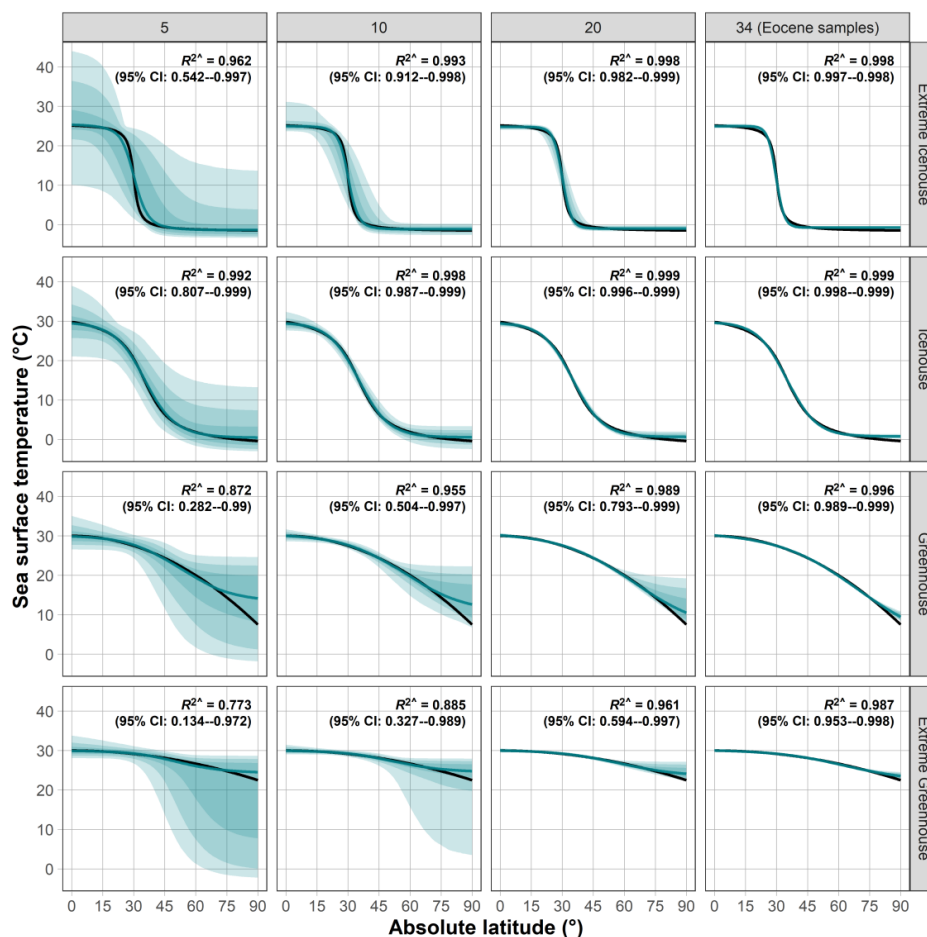


Figure 2: Model reconstructions of simulated latitudinal temperature gradients at various sample sizes. Each column depicts a different reconstruction for given sample sizes: 5, 10, 20, and 34 (latitudes of EECO samples). Each row depicts a different simulated latitudinal temperature gradient that represents idealised climatic states: extreme icehouse, icehouse, greenhouse, and extreme greenhouse. The black line illustrates the simulated gradient. The blue line depicts the reconstructed gradient represented by the median sea surface temperature value estimated from 1,000 model runs with different random samples (first three columns), and a single run with the EECO latitudinal sampling distribution (fourth column). The blue shadings depict the 90%, 95%, and 99% credible intervals. Bold black text within each panel depicts the coefficient of determination (R^2) for estimating goodness of fit between the simulated and modelled gradient. The median (50%) R^2 value along with the 95% credible intervals from all model runs are shown. Each gradient is depicted in absolute latitude.

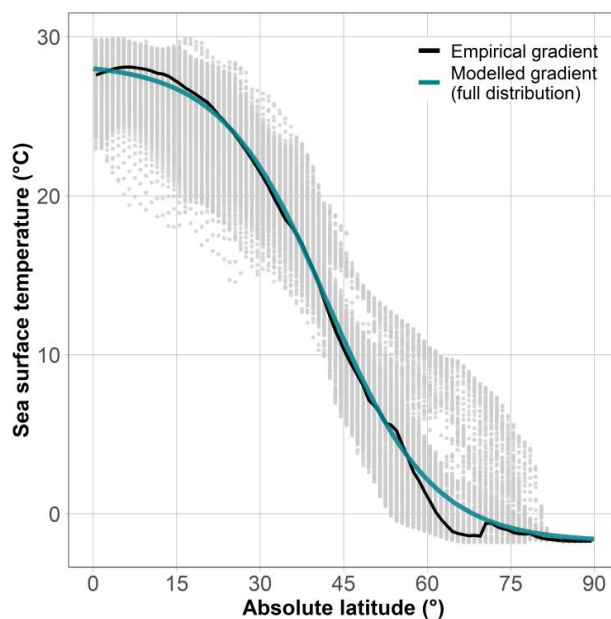


Figure 3: Present-day latitudinal temperature gradient. The present-day empirical latitudinal temperature gradient (median sea surface temperature) is depicted as a black line, and the gradient estimated by the Bayesian model is shown in turquoise. Grey points depict the individual cell values of the Bio-ORACLE grid of mean sea surface temperatures, which were used to infer the empirical and the modelled gradient.

275 Our Bayesian model is able to accurately model a range of idealised temperature gradients, ranging from
276 extreme icehouse to ‘super greenhouse’ scenarios (Fig. 2). Random latitudinal sampling results in highly
277 accurate reconstructions at a sample sizes as low as 10 for the icehouse scenarios (95 % CI of $R^2 > 0.9$).
278 Greenhouse scenarios require additional samples to accurately predict high-latitude temperatures. This is
279 because in the absence of high-latitude samples, the modelled gradient is heavily influenced by the priors,
280 which we based on the modern, the only empirically known latitudinal temperature gradient. A sampling
281 distribution resembling that of the early Eocene data set used in this study allows for a highly accurate
282 reconstruction of even the extreme greenhouse scenario (95 % CI of $R^2 > 0.95$).

283 The average, modern temperature gradient can be closely approximated with our model when using the full
284 modern SST dataset (Fig. 3); almost all of the variation in the empirical median temperatures in bins of 1°
285 absolute latitude is explained by the modelled gradient ($R^2 = 0.997$). The empirical gradient spans 29.3°C
286 from the equator to the poles, the modelled gradient is only slightly higher at 29.6°C. The modern, global
287 mean temperature (GMST) based on our modelled, median gradient is 17.6°C, very similar to the GMST
288 derived from the empirical median gradient (17.5°C).



289 **EECO reconstruction**

290 The modelled Eocene temperature gradient is starkly different from the modern (Fig 4). Modelled, median
291 equatorial temperatures are 4.2 (95% CI: 0.2 – 8.3)°C higher for the EECO, and polar temperatures are 25.0
292 (17.0 – 29.1)°C higher. This results in a flattened latitudinal temperature gradient of 9.0 (2.5 – 17.8)°C for
293 the EECO, as opposed to 29.6°C for the modern. To facilitate the comparison with latitudinal gradients
294 reported in the literature, which sometimes do not report temperatures at very high latitudes, we report also
295 the EECO gradient between the equator and the modern-day polar circle (66.6°), which is slightly lower at
296 7.8 (2.2 – 13.7)°C.

297 The high variability of EECO palaeotemperature proxies, particularly in the mid-latitudes, and the scarcity
298 of high-latitude data, result in substantial uncertainties in the modelled temperature gradient. This is
299 reflected in the residual standard deviation (σ) of the EECO gradient – 4.9 (3.8 – 6.5)°C – which is more
300 than double the σ for the modern gradient, 2.2. This signifies that the early Eocene data does not fit as well
301 to the logistic latitudinal gradient model, which can also be seen from the drastic departure of some of the
302 proxy data from the gradient estimates (Fig. 4).

303 The early Eocene GMST is estimated at 28.7 (26.7 – 30.7)°C, 11.1°C higher than the modern. A model run
304 excluding the ecological proxies increases the GMST by 1.6 (-1.8 – 4.8)°C. The median latitudinal gradient
305 is similar when excluding the ecological proxies, with a median of 9.2°C, but with a 20% wider 95% CI
306 (Fig. S2). This indicates that the ecological proxy data are broadly in agreement with the geochemical
307 proxies, while providing additional constraints on the shape of the early Eocene temperature gradient.

308 Due to the limited spatial coverage of the early Eocene proxy record, and due to the added model complexity
309 of simultaneously estimating a model across both hemispheres, we pooled the proxy data across both
310 hemispheres. Applying the model separately within each hemisphere results in substantial differences in
311 hemispherical, average temperatures, with the Southern Hemisphere being warmer by 6.5 (3.5 – 9.4)°C.
312 The inferred latitudinal gradient is somewhat steeper in the Northern Hemisphere (steeper by 4.8°C,
313 although the 95% CI spans -6.6 – 14.3°C), but the large uncertainties associated with both gradients, and
314 the lack of polar proxy data in the Southern Hemisphere preclude a more precise statement (see Fig. S3).

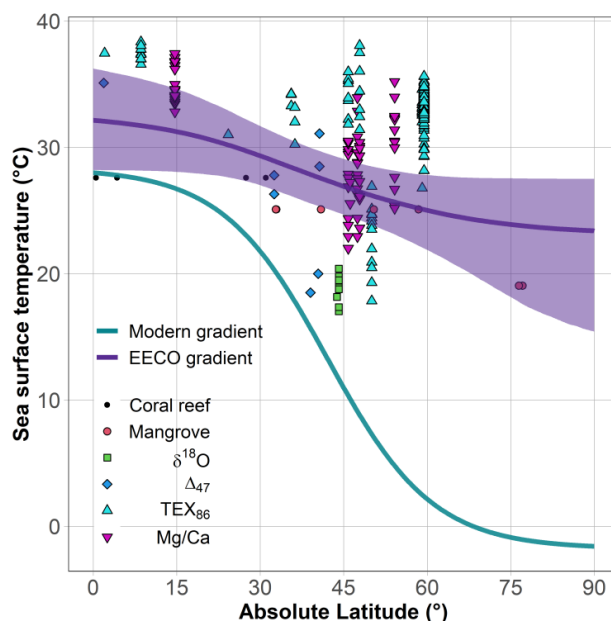


Figure 4: Estimates of the median, latitudinal sea surface temperature gradients of the early Eocene climatic optimum (purple line) and of the present-day (turquoise), both estimated with the Bayesian model. The purple ribbon (shading) depicts the 95% credible interval of the Eocene gradient, the uncertainty of the modern gradient is too low to be visible. Points within the plot depict the geochemical (e.g. TEX_{86}) and ecological (e.g. mangroves) data. Geochemical data are plotted by their point estimate temperature value. Ecological data are plotted at the mean temperature values of their respective normal distributions.

315 Discussion

316 Improved estimation of latitudinal and global palaeotemperatures

317 Our results show that our Bayesian model can be used to reconstruct different types of latitudinal SST
318 gradients from proxy data, even with small sample sizes ($n = 10 - 20$) and patchy sampling distributions
319 (Fig. 2). This is an advancement over previously used linear, quadratic or Gaussian approximations (e.g.
320 Bijl et al., 2009; Tierney et al., 2017), which can fit only specific types of gradients. As such, our model
321 presents an alternative to non-parametric methods for inferring latitudinal temperature gradients, which are
322 sometimes favoured as they can flexibly follow the shape of an unknown temperature gradient (e.g. Zhang
323 et al., 2019; Jones and Eichenseer, 2022). However, when used for interpolation or prediction outside the
324 proxy range, non-parametric methods such as Gaussian process regression strictly respond to the data (e.g.
325 Inglis et al., 2020). This means that the idiosyncrasies of a patchy proxy record, potentially afflicted with



326 measurement errors, calibration errors, and palaeogeographic and temporal uncertainty, dictate the
327 reconstruction of large-scale climate patterns, without the option of including additional knowledge
328 (e.g. that latitudinal temperature gradients should be broadly negative).

329 In contrast, our Bayesian, parametric model allows for the inclusion of informative priors on the model
330 parameters. The modelled sea surface temperature gradient thus does not strictly follow the proxy data, but
331 instead represents a compromise between the data and prior knowledge. In the EECO example (Fig. 4), the
332 inclusion of informative priors improves the prediction of sea surface temperatures in the unsampled, very
333 high latitudes: Notice that the upper limit of the credible interval does not increase beyond the range of the
334 data, whereas unconstrained approaches such as splines, Gaussian processes or even standard linear
335 regression could lead to unrealistically high upper bounds in this case (see Rasmussen and Williams, 2004).
336 Prior information on the shape of latitudinal temperature gradients on Earth exists for all geological time
337 periods. For example, the greater amount of solar radiation per unit area in low latitudes causes Earth's
338 latitudinal temperature gradient to be broadly negative (Beer et al., 2008). The ease with which such prior
339 information can be integrated is a major advantage of our method, as the shape of the modelled gradient is
340 controlled by four parameters which clearly relate to its magnitude, steepness and the latitude of its greatest
341 steepness.

342 Palaeoclimate reconstructions are often summarised as global mean surface temperatures (GMST),
343 providing a standardised metric for characterising the state of the Earth's climate (Royer et al., 2004; Inglis
344 et al., 2020). The calculation of global mean surface temperatures directly from sparse proxy data is
345 susceptible to bias (Jones and Eichenseer, 2022). By modelling the temperature variation across latitudes,
346 a complete temperature distribution along a latitudinal axis can be obtained, filling in gaps in the proxy
347 record through inter- or extrapolation. This eliminates the common problem that specific climate zones
348 dominate the proxy record. Reconstructing the GMST directly from the proxies would lead to an estimate
349 biased towards the well-sampled latitudes. Calculating zonal averages alleviates this problem, but this
350 method relies on comprehensive latitudinal coverage (Inglis et al., 2020). Instead, our method allows for
351 intersecting the modelled temperature gradient at narrow latitudinal intervals, even when significant
352 latitudinal gaps exist. Weighting the temperatures of those latitudinal intervals by area results in GMST
353 estimates without intrinsic spatial biases. We anticipate that this improved method may significantly alter
354 Phanerozoic, proxy-based temperature curves, which have often been directly calculated from the proxy
355 record (Royer et al., 2004; Veizer and Prokoph, 2015). This is particularly relevant for the early Mesozoic
356 and older intervals, for which the spatial coverage is generally poor due to the absence of data from ocean
357 drilling sites (Jones and Eichenseer, 2022).



358 **The role of ecological constraints in palaeoclimate reconstructions**

359 Our results further exemplify how incorporating quantified ecological temperature constraints can provide
360 more precise temperature reconstructions than geochemical proxies alone, adding to the advances in
361 palaeoclimate reconstructions achieved by integrating lithological data (Scotese et al., 2021; Burgener et
362 al., 2023). Combining the occurrences of climate-sensitive plant communities (Greenwood and Wing,
363 1995), reptiles (Markwick, 2007), leaf shapes (Peppe et al., 2011), with geochemical proxies offers
364 substantial potential for improving quantitative palaeoclimate reconstructions across the Phanerozoic. Our
365 modelling framework offers a straightforward, efficient way of integrating ecological climate data with
366 other proxy data: The hierarchical model structure accounts for variation of temperature estimates from
367 proxies at individual localities, which is treated equivalent to the uncertainty associated with the ecological
368 temperature proxies. A local temperature estimate, based on multiple geochemical proxies, thus has the
369 same weight as a local temperature estimate obtained from the occurrence of a climate-sensitive plant
370 community, whilst preserving the uncertainty associated with each estimate. The model could easily be
371 extended to include uncertainties on individual geochemical proxy data, or to variably weight proxy records
372 classified as more or less reliable.

373 Our approach for deriving fully quantitative climate reconstructions from ecological data is borrowed from
374 nearest living relative methods, commonly employed in terrestrial, Cenozoic climate reconstructions
375 (Fauquette et al., 2007; Pross et al., 2012). One major limitation to these methods is that the thermal
376 preferences of taxa may have changed over time. More significantly, in the early Eocene, sea surface
377 temperatures may have reached heights unknown in the modern world, and nearest living relative methods
378 based on the modern are inherently unable to predict such elevated temperatures. This is especially true for
379 taxa that inhabit the warmest part of the ocean today, e.g. coral reefs (Kleypas et al., 1999). Although coral
380 reefs are threatened by warming sea surface temperatures today (Hoegh-Guldberg, 2011), it is conceivable
381 that Eocene reef corals were adapted to a warmer climate. The fossil record indicates that reef development
382 may have been stunted in the early Eocene, with few early Eocene coral reefs occurring in low latitudes
383 (Zamagni et al., 2012). The absence of coral reefs in higher latitudes in the early Eocene could be due to
384 requirements in irradiance, rather than temperature (Muir et al., 2015). Tropical temperatures predicted by
385 the geochemical proxy record indicate hotter-than-modern tropical temperatures for the early Eocene
386 (Fig. S2), suggesting that the modern climate range of coral reefs may underestimate the early Eocene
387 thermal niche for coral reefs. We have tried to account for that possibility by widening the temperature
388 probability distribution for coral reefs, but the predicted temperatures for the reef and mangrove sites still
389 lie below the temperatures indicated by the geochemical proxy record (Fig. 4, Fig. S2).



390 **Early Eocene climate**

391 The geochemical proxy record and ecological data indicate that the latitudinal SST gradient of the early
392 Eocene climatic optimum was significantly shallower than the modern (Huber and Caballero, 2011), but
393 beyond that, there is little agreement. Earlier, reconstructed early Eocene and EECO SST gradients range
394 from 7 – 21°C (Table 1); a more recent reconstruction that includes terrestrial air and sea surface
395 temperatures arrives at a gradient of ~13°C (Inglis et al., 2020). Our polar circle to equatorial gradient
396 estimate is lower than most previous estimates at 7.8°C, although the 95% credible interval extends up to
397 13.7°C and thus overlaps earlier estimates based on shallow water proxies. The confirmation of a very flat
398 gradient by both geochemical and ecological shallow water data indicates that inferred SST gradients based
399 on tropical, shallow water and deep water samples (Cramwinckel et al., 2018; Evans et al., 2018) may
400 overestimate the SST gradient of the early Eocene greenhouse world.

401 Discrepancies between earlier, proxy-based reconstructions and our modelling results are most pronounced
402 in latitudes beyond the polar circle, as earlier approaches (e.g. Tierney et al., 2017) predict almost linearly
403 decreasing SSTs towards the poles, whereas our median prediction suggests only a slight decrease beyond
404 the polar circle. The scarcity of temperature records in this range leads to widening credible intervals in our
405 prediction, including the possibility of stronger temperature decreases. Polar temperature estimates from
406 our model are thus conservative in that they admit large uncertainty where data is absent, which is desirable.
407 However, the presence of high proxy-derived temperature estimates at ~ 60° latitudes forces the modelled
408 median temperature curve to be too high at ~ 24°C, relative to the temperatures indicated by the high-
409 latitude mangrove communities (15.6 - 22.5°C). In contrast, the extrapolated polar temperatures of most
410 previous proxy-based models are likely too low, given the abundance of ecological data indicating
411 temperate or subtropical high-latitude climates during the EECO (Pross et al., 2012; Popescu et al., 2021).

412 The very high variability of the proxy record in mid-latitudes results in large uncertainties on the shape of
413 temperature gradient and on the GMST. Biases and errors in the proxy reconstructions likely contribute to
414 the observed variability, as geochemical proxies reflect many other factors besides seawater temperature
415 (Hollis et al., 2019). Despite excluding $\delta^{18}\text{O}$ measurements from recrystallised fossils, systematic offsets
416 remain between mostly warm temperatures derived from TEX_{86} , and cooler temperatures derived from
417 $\delta^{18}\text{O}$, Δ_{47} , and the ecological proxies. Seasonality (Keating-Bitonti et al., 2011) and temporal changes within
418 the EECO (Westerhold et al., 2018) may also contribute to the large variability of the EECO proxy data.

419 Recent, marine GMST estimates of the EECO and of the early Eocene range from 23.4 – 37.1°C, with the
420 lowest GMSTs being derived from $\delta^{18}\text{O}$, and the higher estimates including TEX_{86} (Inglis et al., 2020).
421 Many studies include both marine and terrestrial proxies to derive GMST estimates, but despite great



422 differences in proxy selection and in the calculation of global average temperatures, many recent estimates
423 fall in the range of 27 - 29.5°C (Hansen et al., 2013; Caballero and Huber, 2013; Cramwinckel et al., 2018;
424 Zhu et al., 2019), similar to our median GMST estimate of 28.7°C.

425 **Conclusions**

426 The Bayesian hierarchical model presented here is able to reconstruct latitudinal gradients from both
427 geochemical and ecological proxy data, while reflecting the uncertainty associated with the ecological
428 temperature proxies, and accounting for the variation of multiple temperature estimates at individual
429 localities. Using informative prior information allows for accurate temperature reconstructions from records
430 with geographically incomplete sampling. By providing temperature estimates across the entire latitudinal
431 range, this method also facilitates the reconstruction of unbiased global average temperatures. Application
432 of our model to the EECO suggests that latitudinal sea surface temperature gradients were shallower than
433 estimated by most previous proxy-based studies. High-latitude pollen records support this interpretation.
434 Our GMST estimate is in good agreement with most existing estimates, indicating that broadly accurate
435 GMST reconstructions are possible even with substantial deviations in the shape of the latitudinal
436 temperature gradient. Our new method opens the door for improving the accuracy of proxy-based
437 palaeoclimate reconstructions and Phanerozoic temperature curves, particularly in intervals with a patchy
438 and unevenly sampled record. Finally, the flexibility of our approach means that estimates can be
439 efficiently updated when new data are made available.

440 **Acknowledgements**

441 The authors are grateful to all those who have enabled this work by collecting, measuring, collating and
442 screening geochemical and fossil data. The contribution of L.A.J. was supported by a Juan de la Cierva-
443 formación 2021 fellowship (FJC2021-046695-I/MCIN/AEI/10.13039/501100011033) from the European
444 Union “NextGenerationEU”/PRTR. For the purpose of open access, the authors have applied a Creative
445 Commons Attribution (CC BY) licence to any Author Accepted Manuscript version arising from this
446 submission.

447 **Author contributions**

448 Both authors designed the study and carried out data preparation. K.E. programmed the model and
449 conducted the analyses. L.A.J. and K.E. generated the figures. Both authors contributed to the writing of
450 the manuscript.



451 **Competing Interests**

452 The authors declare that they have no conflicts of interest.

453 **Data accessibility**

454 The data and code used to produce the results of this study are available via GitHub
455 (<https://github.com/KEichenseer/PalaeoClimateGradient>) and the linked Zenodo repository
456 (<https://zenodo.org/record/7995969>).

457 **References**

- 458 Assis, J., Tyberghein, L., Bosch, S., Verbruggen, H., Serrão, E. A., and De Clerck, O.: Bio-ORACLE v2.
459 0: Extending marine data layers for bioclimatic modelling, *Global Ecology and Biogeography*, 27, 277–
460 284, 2018.
- 461 Beer, J., Abreu, J., and Steinhilber, F.: Sun and planets from a climate point of view, *Proceedings of the*
462 *International Astronomical Union*, 4, 29–43, 2008.
- 463 Bijl, P. K., Schouten, S., Sluijs, A., Reichart, G.-J., Zachos, J. C., and Brinkhuis, H.: Early Palaeogene
464 temperature evolution of the southwest Pacific Ocean, *Nature*, 461, 776–779,
465 <https://doi.org/10.1038/nature08399>, 2009.
- 466 Burgener, L., Hyland, E., Reich, B. J., and Scotese, C.: Cretaceous climates: Mapping paleo-köppen
467 climatic zones using a bayesian statistical analysis of lithologic, paleontologic, and geochemical proxies,
468 *Palaeogeography, Palaeoclimatology, Palaeoecology*, 111373, 2023.
- 469 Burke, K. D., Williams, J. W., Chandler, M. A., Haywood, A. M., Lunt, D. J., and Otto-Bliesner, B. L.:
470 Pliocene and Eocene provide best analogs for near-future climates, *Proceedings of the National Academy*
471 *of Sciences*, 115, 13288–13293, <https://doi.org/10.1073/pnas.1809600115>, 2018.
- 472 Caballero, R. and Huber, M.: State-dependent climate sensitivity in past warm climates and its
473 implications for future climate projections, *Proceedings of the National Academy of Sciences*, 110,
474 14162–14167, 2013.
- 475 Chandra, R., Cripps, S., Butterworth, N., and Muller, R. D.: Precipitation reconstruction from climate-
476 sensitive lithologies using Bayesian machine learning, *Environmental Modelling & Software*, 139,
477 105002, <https://doi.org/10.1016/j.envsoft.2021.105002>, 2021.
- 478 Cramwinckel, M. J., Huber, M., Kocken, I. J., Agnini, C., Bijl, P. K., Bohaty, S. M., Frieling, J., Goldner,
479 A., Hilgen, F. J., Kip, E. L., et al.: Synchronous tropical and polar temperature evolution in the eocene,
480 *Nature*, 559, 382–386, 2018.
- 481 Evans, D., Sagoo, N., Renema, W., Cotton, L. J., Müller, W., Todd, J. A., Saraswati, P. K., Stassen, P.,
482 Ziegler, M., Pearson, P. N., et al.: Eocene greenhouse climate revealed by coupled clumped isotope-mg/ca
483 thermometry, *Proceedings of the National Academy of Sciences*, 115, 1174–1179, 2018.
- 484 Fauquette, S., Suc, J., Jiménez-Moreno, G., Micheels, A., and JOSTS, A.: Latitudinal climatic gradients
485 in the western european and mediterranean regions from the mid-miocene (c. 15 ma) to the, Deep-time



- 486 perspectives on climate change: marrying the signal from computer models and biological proxies, 481,
487 2007.
- 488 Frakes, L. A., Francis, J. E., and Syktus, J. I.: Climate modes of the phanerozoic, 1992.
- 489 Gelman, A., Carlin, J. B., Stern, H. S., Dunson, D. B., Vehtari, A., and Rubin, D. B.: Bayesian data
490 analysis, CRC press, 2013.
- 491 Gelman, A., Goodrich, B., Gabry, J., and Vehtari, A.: R-squared for bayesian regression models, The
492 American Statistician, 2019.
- 493 Gilks, W. R., Richardson, S., and Spiegelhalter, D.: Markov chain monte carlo in practice, CRC press,
494 1995.
- 495 Greenwood, D., Keefe, R., Reichgelt, T., and Webb, J.: Eocene paleobotanical altimetry of victoria's
496 eastern uplands, Australian Journal of Earth Sciences, 64, 625–637, 2017.
- 497 Greenwood, D. R. and Wing, S. L.: Eocene continental climates and latitudinal temperature gradients,
498 Geology, 23, 1044, [https://doi.org/10.1130/0091-7613\(1995\)023<1044:ECCALT>2.3.CO;2](https://doi.org/10.1130/0091-7613(1995)023<1044:ECCALT>2.3.CO;2), 1995.
- 499 Grossman, E. L. and Joachimski, M. M.: Ocean temperatures through the phanerozoic reassessed,
500 Scientific Reports, 12, 8938, 2022.
- 501 Hansen, J., Sato, M., Russell, G., and Kharecha, P.: Climate sensitivity, sea level and atmospheric carbon
502 dioxide, Philosophical Transactions of the Royal Society A: Mathematical, Physical and Engineering
503 Sciences, 371, 20120294, 2013.
- 504 Hoegh-Guldberg, O.: Coral reef ecosystems and anthropogenic climate change, Regional Environmental
505 Change, 11, 215–227, 2011.
- 506 Hollis, C. J., Dunkley Jones, T., Anagnostou, E., Bijl, P. K., Cramwinckel, M. J., Cui, Y., Dickens, G. R.,
507 Edgar, K. M., Eley, Y., Evans, D., et al.: The DeepMIP contribution to PMIP4: Methodologies for
508 selection, compilation and analysis of latest paleocene and early eocene climate proxy data, incorporating
509 version 0.1 of the DeepMIP database, Geoscientific Model Development, 12, 3149–3206, 2019.
- 510 Huber, M. and Caballero, R.: The early eocene equable climate problem revisited, Climate of the Past, 7,
511 603–633, 2011.
- 512 Inglis, G. N., Bragg, F., Burls, N. J., Cramwinckel, M. J., Evans, D., Foster, G. L., Huber, M., Lunt, D. J.,
513 Siler, N., Steinig, S., Tierney, J. E., Wilkinson, R., Anagnostou, E., de Boer, A. M., Dunkley Jones, T.,
514 Edgar, K. M., Hollis, C. J., Hutchinson, D. K., and Pancost, R. D.: Global mean surface temperature and
515 climate sensitivity of the early Eocene Climatic Optimum (EECO), Paleocene (PETM), and latest
516 Paleocene, Climate of the Past, 16, 1953–1968, <https://doi.org/10.5194/cp-16-1953-2020>, 2020.
- 517 Johannes, R., Wiebe, W., Crossland, C., Rimmer, D., and Smith, S.: Latitudinal limits of coral reef
518 growth., Marine ecology progress series. Oldendorf, 11, 105–111, 1983.
- 519 Jones, L. A. and Eichenseer, K.: Uneven spatial sampling distorts reconstructions of Phanerozoic
520 seawater temperature, Geology, 50, 238–242, <https://doi.org/10.1130/G49132.1>, 2022.
- 521 Jones, L. A., Mannion, P. D., Farnsworth, A., Bragg, F., and Lunt, D. J.: Climatic and tectonic drivers
522 shaped the tropical distribution of coral reefs, Nature communications, 13, 1–10, 2022.



- 523 Jones, L. A., Gearty, W., Allen, B. J., Eichenseer, K., Dean, C. D., Galván, S., Kouvari, M., Godoy, P. L.,
524 Nicholl, C., Buffan, L., Flannery-Sutherland, J. T., Dillon, E. M., and Chiarenza, A. A.: palaeoverse: a
525 community-driven R package to support palaeobiological analysis, <https://doi.org/10.31223/X5Z94Q>,
526 2023.
- 527 Judd, E. J., Bhattacharya, T., and Ivany, L. C.: A Dynamical Framework for Interpreting Ancient Sea
528 Surface Temperatures, *Geophysical Research Letters*, 47, e2020GL089044,
529 <https://doi.org/10.1029/2020GL089044>, 2020.
- 530 Judd, E. J., Tierney, J. E., Huber, B. T., Wing, S. L., Lunt, D. J., Ford, H. L., Inglis, G. N., McClymont,
531 E. L., O'Brien, C. L., Rattanasriampaipong, R., et al.: The PhanSST global database of phanerozoic sea
532 surface temperature proxy data, *Scientific data*, 9, 753, 2022.
- 533 Keating-Bitonti, C. R., Ivany, L. C., Affek, H. P., Douglas, P., and Samson, S. D.: Warm, not super-hot,
534 temperatures in the early Eocene subtropics, *Geology*, 39, 771–774, <https://doi.org/10.1130/G32054.1>,
535 2011.
- 536 Kiessling, W.: Paleoclimatic significance of phanerozoic reefs, *Geology*, 29, 751–754, 2001.
- 537 Kleypas, J. A., McManus, J. W., and Meñez, L. A.: Environmental limits to coral reef development:
538 Where do we draw the line?, *American zoologist*, 39, 146–159, 1999.
- 539 Markwick, P.: The palaeogeographic and palaeoclimatic significance of climate, Deep-time perspectives
540 on climate change: Marrying the signal from computer models and biological proxies, 251, 2007.
- 541 Markwick, P. J.: "Equability," continentality, and tertiary "climate": The crocodilian perspective,
542 *Geology*, 22, 613–616, 1994.
- 543 Merdith, A. S., Williams, S. E., Collins, A. S., Tetley, M. G., Mulder, J. A., Blades, M. L., Young, A.,
544 Armistead, S. E., Cannon, J., Zahirovic, S., et al.: Extending full-plate tectonic models into deep time:
545 Linking the neoproterozoic and the phanerozoic, *Earth-Science Reviews*, 214, 103477, 2021.
- 546 Muir, P. R., Wallace, C. C., Done, T., and Aguirre, J. D.: Limited scope for latitudinal extension of reef
547 corals, *Science*, 348, 1135–1138, 2015.
- 548 Peppe, D. J., Royer, D. L., Cariglino, B., Oliver, S. Y., Newman, S., Leight, E., Enikolopov, G.,
549 Fernandez-Burgos, M., Herrera, F., Adams, J. M., et al.: Sensitivity of leaf size and shape to climate:
550 Global patterns and paleoclimatic applications, *New phytologist*, 190, 724–739, 2011.
- 551 Popescu, S.-M., Suc, J.-P., Fauquette, S., Bessedik, M., Jiménez-Moreno, G., Robin, C., and Labrousse,
552 L.: Mangrove distribution and diversity during three Cenozoic thermal maxima in the Northern
553 Hemisphere (pollen records from the Arctic regions), *Journal of Biogeography*, 48, 2771–2784,
554 <https://doi.org/10.1111/jbi.14238>, 2021.
- 555 Pross, J., Contreras, L., Bijl, P. K., Greenwood, D. R., Bohaty, S. M., Schouten, S., Bendle, J. A., Röhl,
556 U., Tauxe, L., Raine, J. I., Huck, C. E., van de Flierdt, T., Jamieson, S. S. R., Stickley, C. E., van de
557 Schootbrugge, B., Escutia, C., and Brinkhuis, H.: Persistent near-tropical warmth on the Antarctic
558 continent during the early Eocene epoch, *Nature*, 488, 73–77, <https://doi.org/10.1038/nature11300>, 2012.
- 559 Quisthoudt, K., Schmitz, N., Randin, C. F., Dahdouh-Guebas, F., Robert, E. M. R., and Koedam, N.:
560 Temperature variation among mangrove latitudinal range limits worldwide, *Trees*, 26, 1919–1931,
561 <https://doi.org/10.1007/s00468-012-0760-1>, 2012.



- 562 Rasmussen, C. E. and Williams, C. K.: Gaussian processes in machine learning, Lecture notes in
563 computer science, 3176, 63–71, 2004.
- 564 Reynolds, R. W. and Smith, T. M.: Improved global sea surface temperature analyses using optimum
565 interpolation, *Journal of climate*, 7, 929–948, 1994.
- 566 Royer, D. L.: Climate reconstruction from leaf size and shape: New developments and challenges, *The*
567 *Paleontological Society Papers*, 18, 195–212, 2012.
- 568 Royer, D. L., Berner, R. A., Montañez, I. P., Tabor, N. J., Beerling, D. J., et al.: CO₂ as a primary driver
569 of Phanerozoic climate, *GSA Today*, 14, 4–10, 2004.
- 570 Salonen, J. S., Korpela, M., Williams, J. W., and Luoto, M.: Machine-learning based reconstructions of
571 primary and secondary climate variables from north american and european fossil pollen data, *Scientific*
572 *reports*, 9, 15805, 2019.
- 573 Schrag, D. P.: Effects of diagenesis on the isotopic record of late paleogene tropical sea surface
574 temperatures, *Chemical Geology*, 161, 215–224, 1999.
- 575 Scotese, C. R., Song, H., Mills, B. J. W., and van der Meer, D. G.: Phanerozoic paleotemperatures: The
576 earth's changing climate during the last 540 million years, *Earth-Science Reviews*, 215, 103503,
577 <https://doi.org/10.1016/j.earscirev.2021.103503>, 2021.
- 578 Sloan, L. C. and Barron, E. J.: "equable" climates during earth history?, *Geology*, 18, 489–492, 1990.
- 579 Song, H., Wignall, P. B., Song, H., Dai, X., and Chu, D.: Seawater Temperature and Dissolved Oxygen
580 over the Past 500 Million Years, *Journal of Earth Science*, 30, 236–243, [https://doi.org/10.1007/s12583-](https://doi.org/10.1007/s12583-018-1002-2)
581 [018-1002-2](https://doi.org/10.1007/s12583-018-1002-2), 2019.
- 582 Suan, G., Popescu, S.-M., Suc, J.-P., Schnyder, J., Fauquette, S., Baudin, F., Yoon, D., Piepjohn, K.,
583 Sobolev, N. N., and Labrousse, L.: Subtropical climate conditions and mangrove growth in Arctic Siberia
584 during the early Eocene, *Geology*, 45, 539–542, <https://doi.org/10.1130/G38547.1>, 2017.
- 585 Taylor, S. P., Haywood, A. M., Valdes, P. J., and Sellwood, B. W.: An evaluation of two spatial
586 interpolation techniques in global sea-surface temperature reconstructions: Last Glacial Maximum and
587 Pliocene case studies, *Quaternary Science Reviews*, 23, 1041–1051,
588 <https://doi.org/10.1016/j.quascirev.2003.12.003>, 2004.
- 589 Tierney, J. E., Sinninghe Damsté, J. S., Pancost, R. D., Sluijs, A., and Zachos, J. C.: Eocene temperature
590 gradients, *Nature Geoscience*, 10, 538–539, 2017.
- 591 Tierney, J. E., Poulsen, C. J., Montañez, I. P., Bhattacharya, T., Feng, R., Ford, H. L., Hönlisch, B., Inglis,
592 G. N., Petersen, S. V., Sahoo, N., et al.: Past climates inform our future, *Science*, 370, eaay3701, 2020.
- 593 Veizer, J. and Prokoph, A.: Temperatures and oxygen isotopic composition of Phanerozoic oceans, *Earth-*
594 *Science Reviews*, 146, 92–104, <https://doi.org/10.1016/j.earscirev.2015.03.008>, 2015.
- 595 Vickers, M. L., Bernasconi, S. M., Ullmann, C. V., Lode, S., Looser, N., Morales, L. G., Price, G. D.,
596 Wilby, P. R., Hougård, I. W., Hesselbo, S. P., et al.: Marine temperatures underestimated for past
597 greenhouse climate, *Scientific reports*, 11, 1–9, 2021.
- 598 Westerhold, T., Röhl, U., Donner, B., and Zachos, J. C.: Global extent of early eocene hyperthermal
599 events: A new pacific benthic foraminiferal isotope record from shatsky rise (ODP site 1209),
600 *Paleoceanography and Paleoclimatology*, 33, 626–642, 2018.



- 601 Yamano, H., Hori, K., Yamauchi, M., Yamagawa, O., and Ohmura, A.: Highest-latitude coral reef at iki
602 island, japan, *Coral Reefs*, 20, 9–12, 2001.
- 603 Zamagni, J., Mutti, M., and Košir, A.: The evolution of mid paleocene-early eocene coral communities:
604 How to survive during rapid global warming, *Palaeogeography, palaeoclimatology, palaeoecology*, 317,
605 48–65, 2012.
- 606 Zhang, L., Hay, W. W., Wang, C., and Gu, X.: The evolution of latitudinal temperature gradients from the
607 latest Cretaceous through the Present, *Earth-Science Reviews*, 189, 147–158,
608 <https://doi.org/10.1016/j.earscirev.2019.01.025>, 2019.
- 609 Zhu, J., Poulsen, C. J., and Tierney, J. E.: Simulation of eocene extreme warmth and high climate
610 sensitivity through cloud feedbacks, *Science advances*, 5, eaax1874, 2019.
- 611 Ziegler, A., Hulver, M., Lottes, A., and Schmachtenberg, W.: Uniformitarianism and palaeoclimates:
612 Inferences from the distribution of carbonate rocks, *Geological journal. Special issue*, 3–25, 1984.